Astrophysical ZeV acceleration in the relativistic jet from an accreting supermassive blackhole Ver. 72

Toshikazu Ebisuzaki[1] and Toshiki Tajima[2]

ebisu@postman.riken.jp

Received _____; accepted _____

to be submitted to Astrophysical Journal Letters

[1]RIKEN, Wako, Saitama, Japan

[2]IZEST: International Center for Zetta- Exawatt Science and Technology

ABSTRACT

An accreting supermassive blackhole, the central engine of active galactic nucleus (AGN), is capable of exciting extreme amplitude Alfven waves whose wavelength (wave packet) size is characterized by its clumpiness. Alfvenic wake-fields excited in the AGN (blazar) jet can accelerate protons/nuclei to extreme energies beyond Zettaelectron volt (ZeV= 10^{21} eV). Such acceleration is prompt, localized, and does not suffer from the multiple scattering/bending enveloped in the Fermi acceleration that causes excessive synchrotron radiation loss beyond 10^{19} eV. The production rate of ZeV cosmic rays is found to be consistent with the observed gamma-ray luminosity function of blazars and their time variabilities.

Subject headings: acceleration of particles — accretion, accretion disks — relativistic processes — galaxies: jets — galaxies: nuclei — gamma rays: galaxies

1. Introduction

The origin of ultra-high energy cosmic rays (UHECRs) with energies 10^{20} eV remains a puzzle of astrophysics. It is generally believed to be extragalactic (Kotera & Olinto (2011), references therein). The production of UHECRs has been discussed mainly in the framework of the Fermi acceleration, in which charged particles gain energy through a numerous number of scatterings by the magnetic clouds. One of the necessary conditions of Fermi acceleration is the magnetic confinement: the Hillas criterion sets a constraint on the product of the magnetic field strength B and extension R of the candidate objects (Hillas criterion; Hillas (1984)): $W \leq W_{\rm max} \sim z(B/1\mu{\rm G})(R/1{\rm kpc})\,{\rm EeV}$, where z is the charge of the particle. The possible candidate objects (but only marginally satisfy the Hillas criterion for 10^{20} eV) are neutron stars, active galactic nuclei (AGN), gamma-ray bursts (GRBs), and accretion shocks in the intergalactic space. However, the acceleration of 10^{20} eV particles even in those candidate objects is not easy for the Fermi mechanism because of 1) a large number of scatterings necessary to reach highest energies, 2) energy losses through the synchrotron emission at the bending associated with scatterings, and 3) difficulty in the escape of particles which are once magnetically confined in the acceleration domain (Kotera & Olinto (2011)).

Tajima & Dawson (1979) first pointed out that intense electromagnetic fields create the plasma wakefield in which charged particles are accelerated by the Lorentz invariant pondermotive force in the longitudinal direction over a long distance. The wakefield acceleration has advantages over the Fermi mechanism in producing UHECRs for the following reasons:

1. The plasma wakefield provides an extremely high accelerating field.

2. It does not require particle bending, which would cause severe synchrotron radiation

losses in extreme energies, because the acceleration field is collinear to the direction of the motion of the accelerated particles.

3. No escape problem exists. Particles can escape from the acceleration region since the wakefield naturally decays out.

In fact the "**wakefield accelerator**" concept is believed to be a promising candidate for a future-generation artificial accelerator (e.g. Leemans (2011)). It has been under intensive research (Esarey et al. (2009)).

Takahashi et al. (2000) and Chen et al. (2002) demonstrated that intense Alfven waves produced by a collision of neutron stars can create wakefields to accelerate charged particles beyond 10^{20} eV. Although such a neutron star collision is believed to be related to short gamma-ray bursts (Nakar (2007)), it is rather rare for two neutron stars to hit each other directly: It requires the same masses, otherwise the tidal field of the more massive star destroys the less massive one to form accretion disk. Chang et al. (2009) conducted one-dimensional numerical simulation showing that whistler waves emitted from an AGN produce wakefields to accelerate UHECR.

The accreting supermassive blackhole, the central engine of an AGN, is one of the candidates for wakefield acceleration. The accretion disk repeats transitions between highly magnetized (low-beta) state and weakly magnetized (high-beta) state (Shibata et al. (1990)). In fact, O'Neill et al. (2011) have found that magnetic transitions with 10-20 orbital periods are predominant in the inner disk through their 3D simulation. Strong pulses of Alfven waves excited in the accretion disk at the transition can create intense wakefields in the relativistic jet launched from the innermost region of the accretion disk. Our analysis finds that these wakefields are natural to accelerate protons and nuclei up to extreme energies of ZeV (10^{21} eV).

In the present paper we carry out a quantitative evaluation of the system of an accreting blackhole which consists of a blackhole itself, an accretion disk, and relativistic jets (figure 1), to lead to the generation of UHECRs beyond 10^{20} eV. The paper is organized as follows. We introduce our model for the intense wakefield generation that is not hampered by the Fermi mechanism limitations in Sec. 2 and find that the highest energy is achievable around an accreting blackhole (AGN) in Sec. 3. Astrophysical implications are discussed in Sec. 4.

2. Intense wakefield mechanism

An accretion disk is formed around a blackhole when gas accretes onto it. Since the angular velocity is higher in inner orbits, there arises a strong shear flow between gases circulating at different radii in the disk. Since the gas is almost fully ionized and Ohmic loss is negligible, magnetic fields are stretched and amplified by the shear motion. The resultant toroidal magnetic field acts as an enhanced friction between gases circulating in the different orbits and transfers the angler momentum outward, while gas is pushed inward because of the reaction of the momentum exchange.

The inner edge of the accretion disk is located around $R = 3R_{\rm g}$, where $R_{\rm g} = 2GM/c^2$ is the gravitational radius of the blackhole. An ergo-sphere appears just outside of causality horizon of the blackhole. The gas inside the ergo-sphere and the outside the horizon can extract the rotational energy from the blackhole, if they are magnetized. They drive relativistic jets in the two axial directions of the accretion disk (Blandford & Znajek (1977)). The Lorentz factor Γ of the bulk motion of the jet is observed as $10 \sim 30$ in the case of active galactic nuclei.

According to Shibata et al. (1990), the accretion disk makes transition between two states: In the weakly magnetized state, a strong shear flow amplifies magnetic fields and

the growth of the magnetic field stops at a certain point and is likely to make transitions between these two states repeatedly. As a result, strong fluctuations are induced in the innermost region of the accretion region ($R < 10R_{\rm g}$). The physical parameters in this innermost region ($R < 10R_{\rm g}$) are estimated according to Shakura & Sunyaev (1973): $\varepsilon_{\rm SS} = 6.6 \times 10^{14} m^{-1}\,({\rm erg\,cm^{-3}})$, $n_{\rm SS} = 2.9 \times 10^{20} \dot{m}^{-2} m^{-1}\,({\rm cm^{-3}})$, $Z_{\rm SS} = 2.2 \times 10^{6} \dot{m} m\,({\rm cm})$, $B_{\rm SS} = 1.8 \times 10^{7} m^{-1/2}\,({\rm G})$, where m is the mass of the blackhole in the unit of solar mass and $\dot{m}$ is the accretion rate normalized to the critical accretion rate ($\dot{M}_c = L_{\rm Edd}/0.06c^2$; Shakura & Sunyaev (1973)). The viscosity parameter α is assumed to be 0.1 in the present paper. From the definition of m and $\dot{m}$, the total luminosity of the accreting blackhole is given by

$$L_{\rm tot} = 1.3 \times 10^{38} m\dot{m} \quad {\rm erg\,s^{-1}}. \tag{1}$$

The wavelength $\lambda_{\rm A}$ of Alfven waves emitted from the accretion disk is calculated as $(V_{\rm A}/C_{\rm s})(\Omega/A)Z_{\rm SS}$ (Matsumoto & Tajima (1995)), where $V_{\rm A}$ is the Alfven velocity in the accretion disk, which is caluculated as: $V_{\rm A} = B_{\rm SS}/\sqrt{4\pi m_{\rm H} n_{\rm SS}}$, and $C_{\rm s}$ is the sound velocity in the accretion disk: $C_{\rm s} = \sqrt{\varepsilon_{\rm SS}/m_{\rm H} n_{\rm SS}}$, where $m_{\rm H}$ is the mass of proton. We assume magnetic field in the accretion disk as $B_{\rm SS}$ and the Keplarian rotation of gas inside the disk, i.e. $\Omega/A = 4/3$. The corresponding angular frequency of the wave is:

$$\omega_{\rm A} = 2\pi c/\lambda_{\rm A} = 3.2 \times 10^{5} \dot{m}^{-1} m^{-1} \qquad {\rm Hz}. \tag{2}$$

The magnetic energy E_B stored in the innermost region of the accretion disk ($R < 10R_g$) is estimated as:

$$E_{\rm B} = (B_{\rm SS}^2/4\pi)\pi(10R_{\rm g})^2 Z_{\rm SS} = 1.6 \times 10^{33} \dot{m} m^2 \quad {\rm erg}. \tag{3}$$

The Alfven waves excited in the accretion disk propagate along the global magnetic field of the jet. The normalized vector potential a is the strength parameter of the wave (Esarey et

al. (2009)) and calculated as:

$$a = \sqrt{2/c}(e/m_{\rm e}c^2)\lambda_{\rm A}\sqrt{B_{\rm SS}^2 V_{\rm A}/4\pi} = 8.3\times10^7\dot{m}^{3/2}m^{1/2}(D/3R_{\rm g})^{-1/2}, \quad (4)$$

where D is the distance from the black hole along the jet. We find that a is much greater than unity for a large class of AGN disks and thus highly relativistic wakefield dynamics is anticipated (Ashour-Abdalla et al. (1981)), where the Alfven flux inside of the jet assumed to be proportional to πb^2 and b to the square root of the distance D: $b = 10R_{\rm g}(D/3R_{\rm g})^{1/2}$. This scaling is consistent with the VLBI observation of the jet of M87, the closest AGN (Asada et al. (2012)). The Lorentz factor of the quivering motion of particles in the wave is of the order of a, i.e., $a \sim \gamma$.

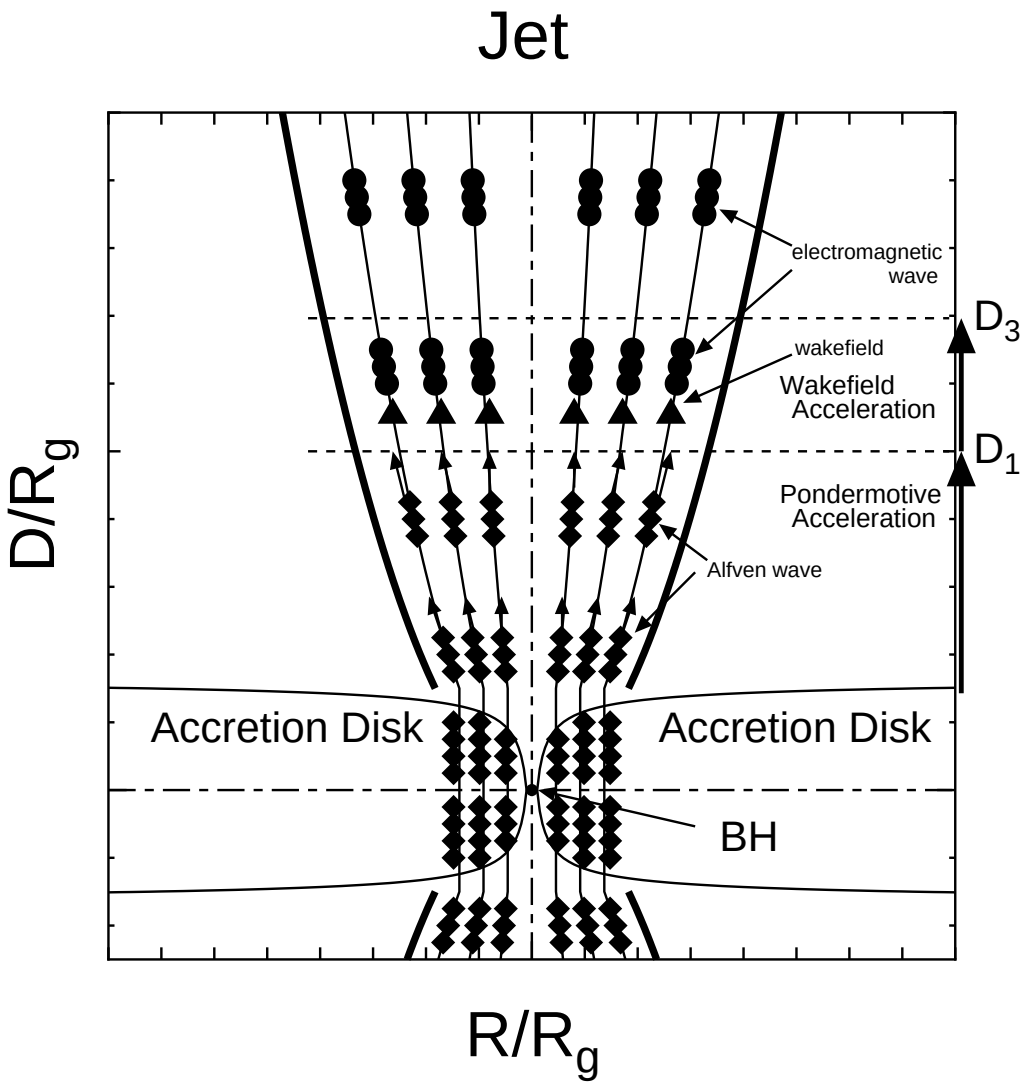

Fig. 1.— Schematic cross section of an disk/jet system around an accreting black hole (BH). Alfven waves (diamonds) are excited in the accretion disk and propagates along the magnetic field (thin solid curves) in the relativistic jet (thick solid curves). They turn into electromagnetic waves (circles) as $\omega_{\rm A}$ approches and exceeds $\omega'_{\rm p}$ and excites wakefields (rectangles) to longitudinally accelerate charged particles (triangles) along the jet.

We focus on the wave modes propagating parallel to the jet magnetic field, since these modes are effective for the linear acceleration to highest energies. The effective plasma frequency $\omega'_{\rm p}$ is estimated as

$$\omega'_{\rm p} = (4\pi n_{\rm J} e^2/m_{\rm e}\gamma\ \Gamma^3)^{1/2} = 6.6\times10^4 \dot{m}^{-1/4} m^{-3/4} (\Gamma/30)^{-2} (\xi/10^{-3})^{1/2} (D/3R_{\rm g})^{-1/4} \quad {\rm Hz}, \tag{5}$$

where the plasma density $n_{\rm J}$ in the jet is calculated through the kinetic luminosity $L_{\rm J}$ of the jet, $L_{\rm J} = n_{\rm J} m_H c^3 \Gamma \pi b^2 = \xi L_{\rm tot}$. On the other hand, the effective cyclotron frequency ω'_c is estimated as

$$\omega'_{\rm c} = eB_{\rm J}/m_{\rm e}c\gamma = 3.8\times10^6 \dot{m}^{-3/2} m^{-1} (D/3R_{\rm g})^{-1/2} \quad {\rm Hz}, \tag{6}$$

where the magnetic field $B_{\rm J}$ in the jet is assumed to be scaled as $B_{\rm J} = B_{\rm SS}(D/3R_{\rm g})^{-1}$:

As an Alfven wave pulse propagates along the jet, the density and magnetic fields decrease, and accordingly the ratios $\omega'_{\rm p}/\omega_{\rm A}$ and $\omega'_{\rm c}/\omega_{\rm A}$ plummet, as seen in figure 2 (for the case of $\dot{m} = 0.1, m = 10^8$ and $\xi = 10^{-3}$). As $\omega'_{\rm p}$ approaches $\omega_{\rm A}$, the whistler branch of the Alfven pulse turns into the electromagnetic wave (Chang et al. (2009)) and start to excite wakefields. The distance D_1 at which $\omega'_{\rm p} = \omega_{\rm A}$ is calculated as:

$$D_1/3R_g = 1.8\times10^{-3} \dot{m}^3 m (\Gamma/30)^{-8} (\xi/10^{-3})^2. \tag{7}$$

Further, $\omega'_{\rm c}$ approaches $\omega_{\rm A}$. In spite of the cyclotron resonance at $\omega'_{\rm c}$, most of the wave energy is likely to tunnel from the whistler branch to the upper branch beyond the right-hand cutoff frequency $\omega_{\rm c}^{\rm rh} = [(\omega'^2_{\rm c} + 4\omega'^2_{\rm p})^{1/2} + \omega'_c]/2$ (which is located above the cyclotron resonance $\omega'_{\rm c}$ in the case of the cold and linear limit [Ichimaru (1973)]). In addition to the linear evanescent tunneling, the nonlinear nature of the EM waves (Ashour-Abdalla et al. (1981); $a \gg 1$) results in the resonance broadening and the nonlinear tunneling.

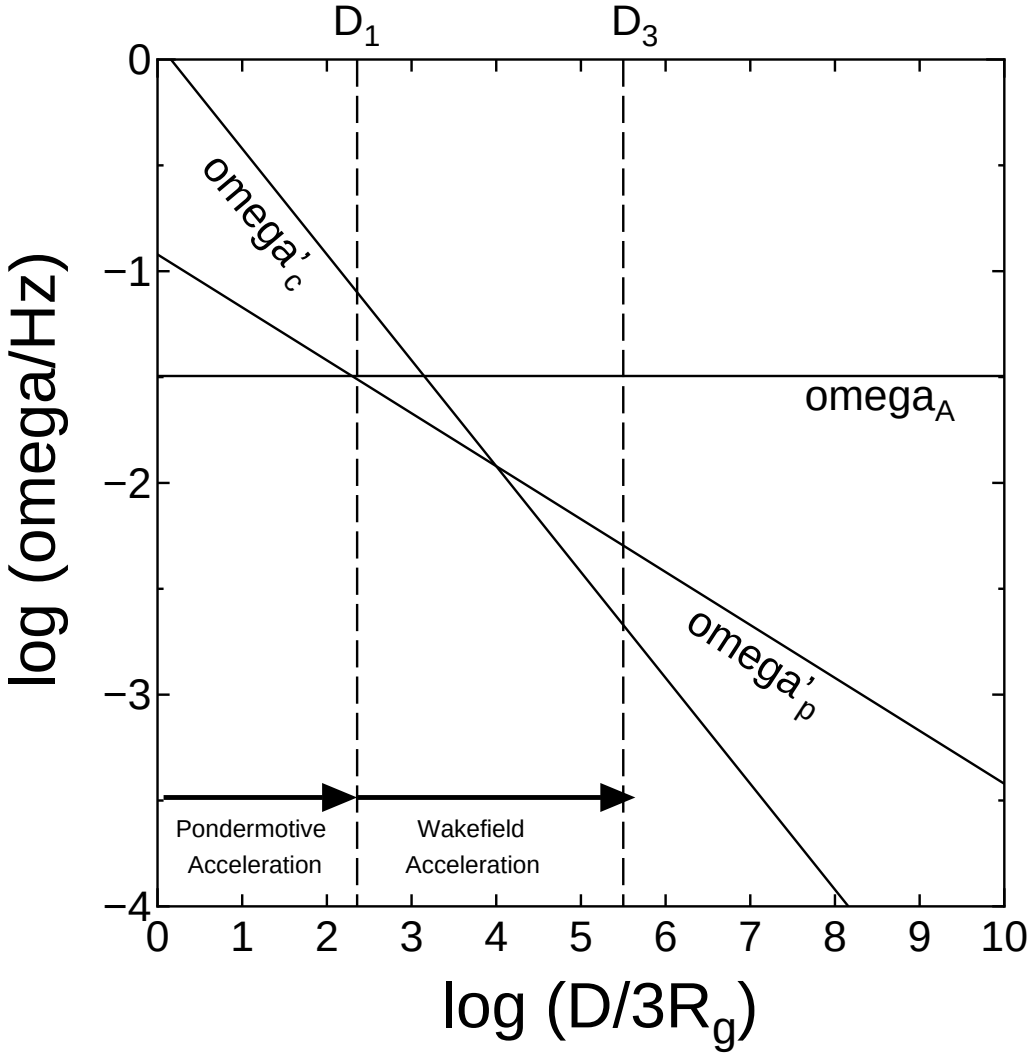

Fig. 2.— Plasma frequency $\omega'_{\rm p}$ and cyclotron frequency $\omega'_{\rm c}$ are plotted against distance D along the jet for the case of $\dot{m} = 0.1$, $\xi = 10^{-3}$, $\Gamma = 30$, and $m = 10^8$. The pulse of Alfven wave with a frequency $\omega_{\rm A}$ is excited in the accretion disk ($D/R_{\rm g} = 1$), propagating along the jet. Both $\omega'_{\rm p}$ and $\omega'_{\rm c}$ decrease as D increases. The Alfven wave (whistler branch) turns itself into electromagnetic pulse around where $\omega'_{\rm p} = \omega_{\rm A}$ and drive wakefields to accelerate charged particles along the jet. Further mode-conversions are possible beyond $\omega_{\rm A} > \omega'_{\rm c}$.

3. Highest energy cosmic rays

Different acceleration mechanisms arise depending on the relative size of $\omega'_{\rm p}$ and $\omega_{\rm A}$. The jet can be divided into two regions, the pondermotive acceleration region ($\omega'_{\rm p} < \omega_{\rm A}$) and the wakefield acceleration region region ($\omega'_{\rm p} < \omega_{\rm A}$).

3.1. Pondermotive accerelation region ($\omega'_{\rm c} > \omega'_{\rm p} > \omega_{\rm A}$)

The phase velocity of Alfven wave in the jet is close to the light velocity because of the small $n_{\rm J}$ compared to $n_{\rm SS}$. In such a case, the particles are accelerated by the pondermotive force parallel to the direction of the propagation of the wave. The maximum energy $W_{\rm PM}$ in the observer's frame of the particles gained in the region is calculated as:

$$W_{\rm PM} = z\Gamma \int_0^{D_1} eE_{\rm PM} dD = 1.1 \times 10^{15} z\dot{m}^2 m (\Gamma/30)^{-1} (\xi/10^{-3}) \quad {\rm eV}, \tag{8}$$

(Ashour-Abdalla et al. (1981)) where $E_{\rm PM} = (m_{\rm e}c/e)a\omega_{\rm A}$ is the pondermotive field of the wave, as far as the acceleration length $Z_{\rm acc} = ca/\omega_{\rm A}$ is greater than D. The distance D_2 is where the acceleration finishes, defined by the equation $D_2 = Z_{\rm pd} = ac/\omega_{\rm A}$. We find that particles arrive at D_1 before D_2: $D_2/3R_{\rm g} = 4.2 \times 10^4 \dot{m}^{5/3} m^{1/3} > D_1/3R_{\rm g}$.

3.2. Wakefiled acceleration region ($\omega'_{\rm p} < \omega_{\rm A}$)

The wakefields of plasma wave are excited in the wakefiled acceleration region and accelerate charged particles. The maximum energy $W_{\rm WF}$ in the observer's frame of the particles gained in the region is calculated as:

$$W_{\rm WF} = z\Gamma \int_{D_1}^{D_3} eE_{\rm WF} dD = 3.3 \times 10^{17} z\dot{m}^{8/5} m^{4/5} (\Gamma/30)^{-3/5} (\xi/10^{-3})^{2/5} \quad {\rm eV}, \qquad (9)$$

(Esarey & Pilloff (1995)) where $E_{\rm WF} = (m_{\rm e}c/e)a\omega'_{\rm p}$ is the maximum electric field in the wakefield. (As commented in section 3.1, this mechanism does not apply for the band $\omega'_{\rm c} < \omega_{\rm A} < \omega_{\rm c}^{\rm rh}$ even when $\omega'_{\rm p} < \omega_{\rm A}$. In equation 9, we neglect this portion for simplicity). It is likely that the acceleration finishes due to the pump depletion $D_3 = Z_{\rm pd} = ac/\omega'_{\rm p}$, where we surmise the interplay between ultrarelativistic wakefield acceleration in the underdense Alfven bubble and the overdense snow-plowing (Ashour-Abdalla et al. (1981)) of plasma ahead of the pulse. This leads to $D_3/3R_{\rm g} = 1.2 \times 10^6 \dot{m}^{7/5} m^{1/5} (\Gamma/30)^{8/5} (\xi/10^{-3})^{-2/5} > D_1/3R_{\rm g}$.

The maximum attainable energy $W_{\rm max}$ can be approximated by $W_{\rm WF}$, since it is always larger than $W_{\rm PM}$ in AGN jets (see equations 8 and 9). The maximum energy $W_{\rm max} \simeq W_{\rm WF}$ is proportional to the 4/5 power of the AGN mass m, as seen in equation 9. We cast this characteristics of the maximum energy gain in AGN wakefields in figure 3. The maximum wakefield energy gain may be upper-bounded by 10^{24} eV at the extreme blackhole mass of $m = 10^{10}$ solar mass. We may set the upper limit of $\dot{m}$ to be around 0.1 for the pondermotive/wakefield acceleration. This is because when $\dot{m}$ approaches unity, the accretion disk becomes radiation dominant so that an Alfven wave pulse becomes weaker than estimated in the present paper.

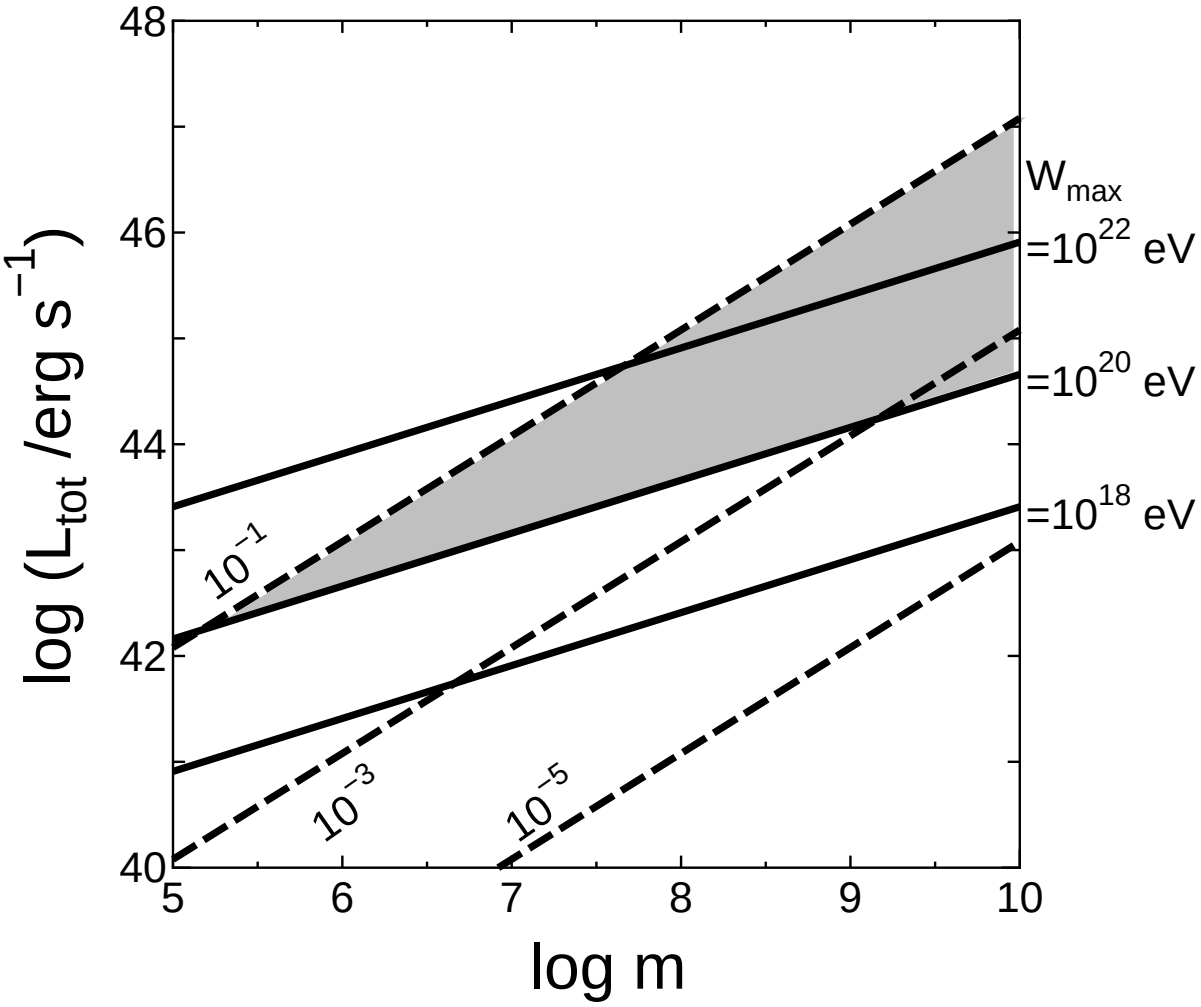

Fig. 3.— The total luminosities of accreting blackholes are plotted against the blackhole mass (in the unit of solar mass) for various maximum attainable energy $W_{\rm max}$ (solid lines) for the case of $\Gamma = 30$ and $\xi = 10^{-3}$. Dashed lines represent the lines for $\dot{m} = 10^{-5}, 10^{-3}$, and 10^{-1}, respectively. The grey triangle represents the parameter sets which allow the acceleration of UHECRs ($\geq 10^{20}$ eV). We may set the uuper limit of $\dot{m}$ to be around 0.1 for the pondermotive/wakefield acceleration may work, since the accretion disk becomes radiation dominant, as $\dot{m}$ approaches unity, so that an Alfven wave pulse becomes weaker than estimated in the present paper.

The energy spectrum of the accelerated charged particles has the power-law with the index of -2 due to the stochasticity arising in the phase matching with the wakefields (Chen et al. (2002)), i.e., $f(W) = A(W/W_{\rm min})^{-2}$. Let κ be the energy conversion efficiency of the acceleration (including the mode convergence efficiency mentioned earlier), then $\kappa E_B = AW_{\rm min}^2 ln(W_{\rm max}/W_{\rm min})$, i.e. $A = 1.6 \times 10^{33} \kappa \dot{m} m^2 [W_{\rm min}^2 ln(W_{\rm max}/W_{\rm min})]^{-1}$. The production rate $\nu_{\rm A}$ of the Alfven wave pulse is estimated as:

$$\nu_{\rm A} = \eta V_A / Z_{SS} = 1.0 \times 10^2 \eta m^{-1} \quad {\rm Hz}, \tag{10}$$

where η is the factor of the order of unity. It is consistent with the 3-dimensional simulations conducted by O'Neill et al. (2011). They found magnetic fluctuations, called Long Period Quasi Periodic Oscillations with the period 10-20 times the Kepler rotation period. The luminosity $L_{\rm UHECR}$ of ultra-high energy cosmic rays is:

$$L_{\rm UHECR} \sim \kappa \zeta E_B \nu_{\rm A} = 1.6 \times 10^{33} (\kappa \zeta / 0.01) \eta \dot{m} m \quad {\rm erg\,s^{-1}}, \tag{11}$$

where $\zeta = ln(W_{\rm max}/10^{20} eV)/ln(W_{\rm max}/W_{\rm min})$.

The wakefields in the jets accelerate both ions and electrons and therefore the AGN jet is likely to be strong gamma-ray sources as well. Although the radiation loss of protons and nuclei is negligible as far as they are accelerated parallel to the magnetic field (Jackson (1963)), that of electrons is likely to be significant, when electrons encounter magnetic fluctuations. The gamma-ray luminosity is, therefore, estimated as:

$$L_\gamma \sim \kappa E_{\rm B} \nu_{\rm A} = 1.6 \times 10^{34} (\kappa / 0.1) \eta \dot{m} m \quad {\rm erg\,s^{-1}}. \tag{12}$$

We summarize the major features of wakefield acceleration in an accreting supermassive blackhole in Table 1.

4. Astrophysical implications and blazar characteristics

Radio galaxies belong to one category of AGN, which has radio lobes connected to the nucleus by relativistic jets. Their central engines are accreting supermassive ($m = 10^6 - 10^{10}$) blackholes. Urry & Padvani (1991) pointed out that they are parent (or misaligned) populations of blazars, which show rapid time variations in many observational bands across radio to gamma rays (10 GeV) with distinct optical and radio polarizations because of their relativistic jet pointing almost toward us. The recent observation by the Fermi satellite reveals that many blazars emit strong gamma-rays in the GeV energy range (Hartman et al. (1999); Ackermann et al. (2011)).

We find that radio galaxies are most likely to be sources of UHECRs and their features fit well with the wakefield theory of acceleration. First, according to Ajello et al. (2012) and Broderick (2012), the local gamma-ray luminosity density of blazars is estimated as $10^{37-38}\mathrm{erg\,s^{-1}(Mpc)^{-3}}$, taking into account the beaming effect of the relativistic jet. Assuming $L_{\rm UHECR}/L_\gamma \sim \zeta \sim 0.1$ (see table 1), the UHECR particle flux becomes: $7.6 \times 10^{-2}\, l_{\gamma 37}(\zeta/0.1)(\tau_8/1.5)$ [particles/(100 km^2 yr sr)]. This is consistent with observed flux of UHECR. Here, $l_{\gamma 37}$ is the local gamma-ray luminosity density of blazars in the unit of $10^{37}\mathrm{erg\,s^{-1}\,(Mpc)^{-3}}$ and τ_8 is the life time of UHECR particles (in the unit of 10^8yr), which is determined by GZK process: Greisen (1966) and Zatsepin & Kuzmin (1966) predicted that cosmic-ray spectrum has a theoretical upper limit around 5×10^{19} eV, because of the opening of the channel to produce Δ^+ particles, which decay into pions (π^0 and $\pi^\pm$) and further into photons, electrons, protons, neutrons, and neutrinos.

Second, blazars are also known for being highly variable at all wavelengths and all time scales. In the most extreme cases, the timescales of gamma-ray variability can be as short as a few minutes at very high energies ($\sim$ 100 GeV; VHE). Such variability has been detected in several BL Lacertae objects (Arlen et al. (2013); Gaido et al. (1996); Albert et

Table 1: Major features of wakefield acceleration in an accreting supermassive blackhole.

	values	units
$2\pi/\omega_{\rm A}$	$2.0\times10^{2}(\dot{m}/0.1)(m/10^{8})$	s
$1/\nu_{\rm A}$	$1.0\times10^{6}\eta^{-1}(m/10^{8})$	s
D_2/c	$5.6\times10^{9}(\Gamma/30)^{8/5}(\xi/10^{-3})^{-2/5}(\dot{m}/0.1)^{7/5}(m/10^{8})^{6/5}$	s
$W_{\rm max}$	$2.2\times10^{22}z(\Gamma/30)^{-3/5}(\xi/10^{-3})^{2/5}(\dot{m}/0.1)^{8/5}(m/10^{8})^{4/5}$	eV
$L_{\rm tot}$	$1.2\times10^{45}(\dot{m}/0.1)(m/10^{8})$	$\rm erg\,s^{-1}$
$L_{\rm A}$	$1.2\times10^{42}\eta(\dot{m}/0.1)(m/10^{8})$	$\rm erg\,s^{-1}$
L_{γ}	$1.2\times10^{41}(\eta\kappa/0.1)(\dot{m}/0.1)(m/10^{8})$	$\rm erg\,s^{-1}$
$L_{\rm UHECR}$	$1.2\times10^{40}(\eta\kappa\zeta/10^{-2})(\dot{m}/0.1)(m/10^{8})$	$\rm erg\,s^{-1}$
$L_{\rm UHECR}/L_{\rm tot}$	$1.0\times10^{-5}(\eta\kappa\zeta/10^{-2})$	-
$L_{\rm UHECR}/L_{\gamma}$	$1.0\times10^{-1}(\zeta/0.1)$	-

$\xi = L_{\rm J}/L_{\rm tot}$, $\eta = \nu_A Z_{\rm SS}/V_{\rm A}$, $\kappa = E_{\rm CR}/E_{\rm A}$, and $\zeta = ln(W_{\rm max}/(10^{20}eV))/ln(W_{\rm max}/W_{\rm min})$.

al. (2007); Aharonian et al. (2007); Aleksic et al. (2011); Saito et al. (2013)). On the other hand, the wakefield acceleration mechanism predicts the rapid time variability with all the time scales from the Alfven frequency ($2\pi/\omega_{\rm A} \sim 100\,{\rm s}$), through the repetition period of the pulses ($1/\nu_{\rm A}$ ∼days), and to the propagation time in the jet ($D_2/c, 1 \sim 10^3\,{\rm years}$). This time variability is both for ion acceleration variability for UHECRs as well as electron variability as observed in gamma rays (electron energies are limited by the radiation energy loss by PeV (Deng et al. (2012)). The finer structure of time variability is anticipated from our mechanism, as the magnetic structure may contain finer structure of braiding within the above quoted Alfven pulse. These observed blazar variabilities are the natural consequences deeply embedded in our model.

Third, the multiple epoch observation of VLBA provides a strong evidence that gamma-ray emission comes from parsec scale jet (Lister et al. (2009); Marscher et al. (2010); Lyutikov & Lister (2011)). Since the life time of high energy electrons is much shorter than the propagation time, they must be locally accelerated. This is consistent with the picture of the wakefield acceleration, since a swarm of the electrons is accelerated locally in the wakefields propagating in the jets. They are likely to emit a highly variable and polarized gamma-rays due to their high gamma-factor.

Our calculation shows the UHECR flux of a gamma-ray emitting galaxy as:

$$F_{\rm UHECR} = 3.5\times10^{-1}(\zeta/0.1)(F_\gamma/10^{-8}\,{\rm photons\,cm^{-2}\,s^{-1}})(\overline{E_\gamma}/1\,{\rm GeV}) \quad {\rm particles}/(100\,{\rm km^2\,yr})^{-1}, \tag{13}$$

if the radiation pattern of UHECRs is the same as that of gamma-rays. Here, F_γ is the gamma-ray flux and $\overline{E_\gamma}$ is the average gamma-ray energy. This value is large enough to be identified as an individual source by a cluster of events with a next generation space borne detector of UHECR, like JEM-EUSO, which can achieve an integrated exposure of $10^6\,{\rm km^2\,str\,yr}$ (Takahashi et al. (2008); Kajino et al. (2009); Gorodetzky (2011)). On the

other hand, the flux of the cosmogenic neutrinos, produced by the GZK process is as high as $5.4 \times 10^{-1}\, l_{\gamma 37}(\zeta/0.1)(\tau/100)\,[\mathrm{particles}/(100\,\mathrm{km}^2\,\mathrm{yr\,sr})]$, assuming the conversion efficiency of UHECR to UHEν to be 10%. This is consistent with the previous works for the case of $W_{\max} = 10^{21.5}$ (e.g. Kotera et al. (2010)). JEM-EUSO can also detect this level of UHEν flux as well (Santangelo et al. (2010)).

5. Conclusions

We have introduced the wakefield acceleration mechanism arising from the Alfvenic pulse incurred by an accretion disk around an supermassive blackhole, the central engine of AGN. This provides a natural account for UHECRs, and also the accompanying gamma-rays and their related observational characteristics, such as their luminosities, time variations, and structures. The severe physical constraints in the extreme ZeV energies by the Fermi acceleration have been lifted by the present mechanism. We have identified a number of areas of future research that needs further studies, including the bubble dynamics of superintense Alfven pulses in 1-3 dimensions.

We would like to dedicated this paper to the late Professor Yoshiyuki Takahashi, whose encouragement on this work has been crucial.

REFERENCES

Ajello, M. et al. 2012, ApJ, 751, 108

Ackermann, M., Ajello, M., Allafort, A., et al. 2011, ApJ, 743, 171

Aharonian, F., Akhperjanian, A. G., Bazer-Bachi, A. R., et al. 2007, ApJ, 664, L71

Albert, J., Aliu, E., Anderhub, H., et al. 2007, ApJ, 666, L17

Aleksic, J., Antonelli, L. A., Antoranz, P., et al 2011, ApJ, 730, 8

Arlen, T. et al. 2013, ApJ, 762, 92

Asada, K. and Nakamura, M. 2012, ApJ, 745, L28

Ashour-Abdalla, M., Lebouf, J.N., Tajima, T., Dawson, J. M., and Kennel, C. F., 1981, Phys. Rev. A. 23, 1906

Blandford, R. D. and Znajek, R. L. 1977, MNRAS, 179, 433

Broderick, A.E. 2012, ApJ, 752, 22

Chang, F.Y. et al. 2009, Phys. Rev. Lett. 102, 111101

Chen, P.C., Tajima, T., and Takahashi, Y. 2002, Phys. Rev. Lett. 89, 161101

Deng, A. et al., 2012, Phys. Rev. STAB 15, 081303

Esarey, E. and Pilloff, M. 1995, 2, 1432

Esarey, E., Schroeder, C.B., and Leemans, W.P. 2009, Rev. Mod. Phys., 81, 1229

Fermi, E., 1954 ApJ, 119, 1

Gaidos, J. A., Akerlof, C. W., Biller, S., et al. 1996 Nature, 383, 319

Gorodetzky P. et al. 2011, Nucl. Inst. & Meth. in Phys. Res. Sect. A, 626, S40.

Greisen, K., Phys. Rev. Let. 1966, 16, 748

Hartman, R. C., Bertsch, D. L., Bloom, S. D., et al. 1999, ApJS, 123, 79

Hillas, A. M., 1984, Ann. Rev. Astron. Astrophys., 22, 425

Ichimaru, S., 1973, Basic Principle of Plasma Physics, Benjamin, Reading, p.89

Jackson, J.D. 1963, Classical Electrodynamics, John Wiley and Son.

Kajino, F. et al. 2009, Nuclear Instruments & Methods, 1, 422

Kotera, K., Allard, D., and Olinto, A., 2010, J. of Cosmology & Astroparticle Physics, 10, 013

Kotera, K. and Olinto, A. 2011, Ann. Rev. Astron. Astrophys., 49, 119

Leemans, W. 2011, in ICFA Beam Dynamics Newsletters, 56, 10

Lister, M. L., et al. 2009, AJ, 137, 3718

Lyutikov, M. and Lister, M. 2010, ApJ, 722, 197

Marscher, A. P., & Jorstad, S. G. 2010, ApJ, 710, L126

Matsumoto, R. and Tajima, T., 1995, ApJ, 445, 767

Nakar, E., 2007, Phys. Rep. 442, 166

O'Neill, S.M., et al. 2011, ApJ, 736, 107

Saito, S. et al. 2013, ApJ, 766, L11.

Santangelo, A. 2010, Progress in Particle and Nuclear Physics, 64, 366

Shakura, N.I. and Sunyaev, R.A. 1973, A&A, 24, 337

Shibata, K., Tajima, T., and Matsumoto, R., 1990, ApJ, 350, 295

Tajima, T. and Dawson, J. M., Phys. Rev. Lett. 1979, 43, 267

Takahashi, Y., Tajima, T., and Hillman, L. 2000, in High Field Science, eds. T. Tajima, K. Mima, and H. Baldis, Klewer, p. 171

Takahashi, Y. et al. 2008, New J. of Phys., 11, 065009

Takahara, F. Prog. Theor. Phys. 1990, 83, 1071

Urry, C.M., & Padovani, P. 1991, ApJ, 371, 60

Zatsepin, G.T. and Kuzmin, V.A. 1966, JETP Lett. 4, 78